

# Different facets of the raise and peel model

**Francisco C. Alcaraz<sup>1</sup> and Vladimir Rittenberg<sup>2,3</sup>**

<sup>1</sup>Instituto de Física de São Carlos, Universidade de São Paulo, Caixa Postal 369, 13560-590, São Carlos, SP, Brazil

E-mail: [alcaraz@if.sc.usp.br](mailto:alcaraz@if.sc.usp.br)

<sup>2</sup>Physikalisches Institut, Bonn University, 53115 Bonn, Germany

<sup>3</sup> Department of Mathematics and Statistics, University of Melbourne, Parkville, Victoria 3010, Australia

E-mail: [vladimir@th.physik.uni-bonn.de](mailto:vladimir@th.physik.uni-bonn.de)

## **Abstract.**

The raise and peel model is a one-dimensional stochastic model of a fluctuating interface with nonlocal interactions. This is an interesting physical model, in this paper we review its properties. It's phase diagram has a massive phase and a gapless phase with varying critical exponents. At the phase transition point, the model exhibits conformal invariance which is a space-time symmetry. Also at this point the model has several other facets which are the connections to associative algebras, two-dimensional fully packed loop models and combinatorics.

*Keywords:* conformal field theory, avalanches(theory), stochastic processes, special issue

## 1. Introduction

The raise and peel model (RPM), reviewed in this paper, is a one-dimensional adsorption-desorption model of a fluctuating interface [1, 2]. The interface evolves following nonlocal Markovian dynamics. Originally, the model "appeared" [3] during an investigation of some intriguing connections between the groundstate wavefunctions of the XXZ quantum chain and two-dimensional dense  $O(n = 1)$  fully packed loop models [4, 5]. For some special boundary fully packed loop (FPL) models [6, 7] are related [8] to Alternating Sign Matrices [9], which are of interest in combinatorics. These magic connections were found by Razumov and Stroganov [10]-[12].

The stationary states probability distribution functions (PDF) of the RPM are given precisely by the Razumov-Stroganov wavefunctions. It was later understood that the RPM is in fact a very interesting model on its own. Moreover, objects with a nice mathematical structure, and this indeed the case of Razumov-Stroganov wavefunctions, allow, using small systems sizes, to make conjectures for the expression of physical quantities for any systems sizes.

The RPM is not only special because of the nice properties of the stationary states PDF but also for its dynamics. For large system sizes, the finite-size scaling eigenspectrum of the Hamiltonian describing the continuous time evolution of the RPM is expressed in terms of characters of the Virasoro algebra [13], hence conformal invariance (this implies that the dynamical critical exponent has the value  $z = 1$ ). To our knowledge, the RPM is the first known example of a stochastic process having this space-time symmetry. As we are going to see, this symmetry has consequences for the physical properties of the model including the stationary states.

By changing the ratio of the adsorption and desorption rates of the model, the RPM can be taken away from the Razumov-Stroganov point (which corresponds to the case where the rates are equal). We show the phase diagram of the model thus obtained. If the adsorption rates exceed the desorption rates, one gets a gapless phase with continuously varying critical exponents. If the desorption rates are higher than the adsorption ones, the system is massive (finite correlation lengths).

The presentation of the different facets of the RPM will be kept as elementary as possible, for the reader who wants to know more, we give references.

In Section 2 we give a connection between associative algebras and stochastic processes. This connection is important since the structure of the RPM and some of its extensions are related to the Temperley-Lieb (TL) algebra [14, 15] and its extensions [8]. Moreover one can use two representations of the TL algebra. One in terms of RSOS paths which is useful for the interface model and another one in terms of up and down spins. In the latter representation, one gets a quantum spin chain Hamiltonian which is integrable and therefore the spectrum can be computed exactly using the Bethe ansatz. In Section 3 we give the finite-size scaling limit of the Hamiltonian eigenspectrum. It is at this point that conformal invariance enters the picture.

In Section 4 we show how the Hamiltonian expressed in terms of the generators of

the TL algebra acts in the representation given by link patterns (equivalent to RSOS paths). We consider the example of a Hamiltonian containing 5 generators acting in a space of 5 link patterns configurations. We compute the PDF of the stationary state (ground-state wavefunction) and show how it can be related to the 26 configurations of a fully packed loop model (FPL) on a rectangle or to 26 vertically symmetric alternating sign matrices. This phenomenon which is valid not only for the case of five generators, is very interesting since it relates the stationary state of a one-dimensional stochastic process to an equilibrium two-dimensional system. This is the Razumov-Stroganov conjecture.

All these considerations were valid for the RPM at the Razumov-Stroganov point. In Section 5 we describe the one-parameter dependent RPM. The parameter denoted by  $u$  is the ratio of the adsorption to desorption rates. For  $u$  not equal to one, the model is not anymore related to the TL algebra, few analytic calculations are possible and the study is based on Monte-Carlo simulations. We give the phase diagram of the model which is based on the results given in the next sections.

In Section 6 we give the properties of the stationary states, stressing what is special for the case  $u = 1$ . Section 7 deals with the dynamics of the model. Since the desorption processes are not local, avalanches occur. We briefly mention their properties.

Some results not described in this paper are briefly presented in Section 8. We also list some open questions.

## 2. Markovian dynamics and associative algebras.

The continuous time evolution of a system composed by the states  $a = 1, 2, \dots, N$  with probabilities  $P_a(t)$  is given by a master equation that can be interpreted as an imaginary time Schrödinger equation:

$$\frac{d}{dt}P_a(t) = - \sum_b H_{a,b}P_b(t), \quad (1)$$

where the Hamiltonian  $H$  is an  $N \times N$  intensity matrix:  $H_{a,b}$  nonpositive ( $a \neq b$ ) and  $\sum_a H_{a,b} = 0$ .  $-H_{a,b}$  is the rate for the transition  $|b\rangle \rightarrow |a\rangle$ . The ground-state wavefunction of the system  $|0\rangle$ ,  $H|0\rangle = 0$ , gives the probabilities in the stationary state:

$$|0\rangle = \sum_a P_a |a\rangle, \quad P_a = \lim_{t \rightarrow \infty} P_a(t). \quad (2)$$

The normalization factor of the unnormalized probabilities  $P_a$  is  $\langle 0|0\rangle$  where

$$\langle 0| = \sum_a \langle a|, \quad \langle 0|H = 0. \quad (3)$$

Since  $H$  is an intensity matrix the real parts of the  $N$  eigenvalues  $E(k)$  are nonnegative and, if complex, the eigenvalues come in conjugate pairs. The eigenvalue zero is not degenerate. Conversely, if the spectrum of a matrix has these properties, through similarity transformations the matrix can be brought to the form of intensity matrices (the solutions are not unique).

Let us now consider an associative algebra with generators  $A(i)$  ( $i = 1, 2, \dots, m$ ). Taking products of the generators one gets the words  $w(r)$ . The algebra is defined by giving some relations between the words. If we can choose the independent words  $W(r)$  such that any product of them verify the relation:

$$W(r)W(s) = \sum_q p_q^{r,s} W(q), \quad p_q^{r,s} \geq 0, \quad \sum_q p_q^{r,s} = 1, \quad (4)$$

then the Hamiltonian

$$H = \sum_u a(u)(1 - W(u)), \quad (5)$$

acting in the vector space defined by the basis of independent words  $W(s)$ , is an intensity matrix if the coefficients  $a(u)$  are nonnegative.  $H$  is acting from the left on the words  $W(s)$  of the vector space:  $W(u)W(s)$  ( $W(u)$  is one on the terms in (5) and  $W(s)$  belongs to the vector space). The action of the independent words  $W(u)$  on the vector space defined by the same words gives the regular representation of the algebra.

If the algebra  $A$  contains a left ideal‡ defined by the words  $I_A$ , the Hamiltonian (5) acting on this ideal gives again a stochastic process. If  $A$  has several ideals  $I_1(I_2(\dots(I_n, H$  has a block triangular form. The ground-state wavefunction  $|0\rangle$  is a linear combination of the states (words) which define the vector space  $I_1$ . These states are also called recurrent states. The words belonging to the ideals  $I_2, \dots, I_n$  but not belonging to  $I_1$  do not appear in the stationary state.

We will give a simple example. Consider the Abelian algebra given by  $m$  generators  $A(i)$  ( $i = 1, 2, \dots, L$ ) satisfying the relations:

$$A(i)^2 = aA(i+1)^2 + bA(i)A(i+1), \quad i = 1, 2, \dots, L-1, \quad (6)$$

$$A(L)^2 = a + bA(L), \quad (7)$$

where

$$[A(i), A(j)] = 0, \quad i, j = 1, \dots, L, \quad a + b = 1, \quad a, b \geq 0. \quad (8)$$

The model is defined by the Hamiltonian:

$$H = 1 - \frac{1}{L} \sum_{i=1}^L A(i). \quad (9)$$

$H$  acts in the  $2^L$  dimensional vector space of independent words which is given by the monomials:  $1, A(i), A(i)A(j)$  ( $i \neq j$ ), .... The physical interpretation of the vector space is obvious. Take a one-dimensional system with  $L$  sites. Each site can be empty or occupied by at most one particle. In the state  $A(i_1)A(i_2)\dots A(i_k)$  the site  $i_n$  is occupied if  $A(i_n)$  appears in the expression of the monomial. In this sandpile model (see Dhar's papers [16] for much more on this subject), the toppling mechanism is encoded in the algebra (6)-(8) and the dynamics in Eq. (9). In a unit of time a particle is introduced with probability  $1/L$  at any site of the lattice (see Eq. (9)). Without increasing the time, a given site  $i$  with more than a single particle, has the probability  $a$  (probability

‡ A left  $I_A$  ideal of an algebra  $A$  is a subspace of  $A$  such that  $aX \in I_A$  for all  $a \in A$  and  $X \in I_A$ .

*b*) of sending two (one) of its particles to the site  $i + 1$  (see Eq. (6)). Particles at the site  $L$  may leave the lattice (see Eq. (7)). The process continues up to when we have at most a single particle in any lattice point.

A special class of associative algebras in which the condition (4) is satisfied are semigroup algebras. In this case, the relations (4) take the simple form:

$$U(q) = W(s). \quad (10)$$

An important example of this kind is the Temperley-Lieb (TL) algebra with the generators  $e_j$  ( $j = 1, \dots, L - 1$ ) satisfying:

$$e_j^2 = (q + q^{-1})e_j, \quad e_j e_{j \pm 1} e_j = e_j, \quad e_j e_k = e_k e_j \quad \text{for } |j - k| > 1, \quad (11)$$

with  $q$  having the special value  $q = \exp(i\pi/3)$ . The special choice in (5) where we take  $a(u) = 1$  and for  $W(u)$  only the generators  $e_j$  gives the exact integrable quantum Hamiltonian

$$H = \sum_{j=1}^{L-1} (1 - e_j). \quad (12)$$

For other values of  $q$ , the relations (11) define an associative algebra but not a semigroup. The TL semigroup (11) can be generalized in several ways. One can add boundary generators [17]-[20] or one can generalize the group algebra itself. Examples of the latter are the multi-colored versions of the TL semigroup [21, 22] or the rotor model [23]. Physical applications of these models have not yet been studied.

Another important example of a semigroup with possible applications to stochastic processes is the Brauer semigroup algebra [24, 25, 26].

In all these cases, the unnormalized probabilities  $P_a$  which appear in the ground-state wavefunction  $|0\rangle$  are positive numbers. If these numbers are integer multiples of the lowest one, they might have a combinatorial meaning and the challenge is to find and understand them.

From now on we will study only the applications of the TL semigroup defined by Eq. (11) and take the Hamiltonian (12) with  $L$  an even number ( $L = 2n$ ).

One has to specify the vector space in which the Hamiltonian (12) acts. The TL algebra has a left ideal  $I_1$  defined by the words [15, 5]

$$W(s)J_0, \quad J_0 = \prod_{j=1}^{L/2} e_{2j-1}, \quad (13)$$

where  $W(s)$  is any word of the algebra. There are

$$C_n = \frac{1}{n+1} \binom{2n}{n} \quad (14)$$

words in this ideal. For example, if  $L = 4$ , the two independent words in this left ideal are:  $e(1)e(3)$  and  $e(2)e(1)e(3)$ . In Section 4 we discuss in detail the action of  $H$  in this vector space. The raise and peel model at the Razumov-Stroganov point is defined by the Hamiltonian (12) acting on this ideal.

As opposed to the Abelian algebra (6)-(8) or other Abelian sandpile models, it is not clear at all how the TL algebra which is not Abelian can be related to a toppling process.

There is another useful (reducible) representation of the TL semigroup in a spin basis. The matrices

$$e_j = \frac{1}{2}[\sigma_j^x \sigma_{j+1}^x + \sigma_j^y \sigma_{j+1}^y - \frac{1}{2} \sigma_j^z \sigma_{j+1}^z + i \frac{\sqrt{3}}{2}(\sigma_j^z - \sigma_{j+1}^z)], \quad (15)$$

where  $\sigma^x, \sigma^y$  and  $\sigma^z$  are Pauli matrices, satisfy (11). The Hamiltonian given by (12) becomes a spin 1/2 quantum spin chain acting in a  $2^L$  dimensional vector space. It is known that this reducible representation contains all the irreducible representations of the TL algebra, in particular the one given by the left ideal discussed above.

### 3. The raise and peel model and conformal invariance

The quantum spin chain defined by the Hamiltonian (12) and (15) commutes not only with

$$S^z = \frac{1}{2} \sum_{j=1}^L \sigma_j^z, \quad (16)$$

but with two other operators  $S^+$  and  $S^-$  (see [27]). The three operators  $S^z$ ,  $S^+$  and  $S^-$  which are related by commutation relations define the quantum algebra  $U_q(sl(2))$  for  $q = \exp(i\pi/3)$ . This is a deformation of the usual angular momentum  $sl(2)$  algebra with irreducible representations of dimension  $2s + 1$  labeled by the spin  $s$  (integer or half integer). The number of scalars ( $s = 0$  representations) for a chain with  $L = 2n$  sites is given by the Catalan numbers (14) which coincide with the number of states in the left ideal given by (13). It can be shown that this is not a simple coincidence. The spectrum of the Hamiltonian defined in this left ideal is obtained considering only the scalar sector of the quantum spin chain.

The quantum spin chain is an integrable system [28]. This implies that it's spectrum can be computed exactly using the Bethe ansatz. If we denote by  $E_r$  ( $r = 0, 1, \dots, 2^L$ ) the energy levels in nondecreasing order:  $E_0 = 0 < E_1 \leq E_2 \leq \dots$ , the finite-size scaling partition function of  $H$  is defined as follows :

$$Z(q) = \lim_{L \rightarrow \infty} Z_L(q) = \lim_{L \rightarrow \infty} \sum_n q^{LE_n/\pi v_s}, \quad (17)$$

where  $v_s = 3\sqrt{3}/2$  is the sound velocity [28]. One can show [29] that  $Z(q)$  has the expression

$$Z(q) = \sum_s (2s + 1) \zeta_s(q). \quad (18)$$

Here  $s$  is the spin, taking the values  $s = 0, 1, 2, \dots$ , for  $L$  even, and  $s = \frac{1}{2}, \frac{3}{2}, \frac{5}{2}, \dots$ , for  $L$  odd, and

$$\zeta_s(q) = q^{\Delta_s} (1 - q^{2s+1}) \prod_{n=1}^{\infty} (1 - q^n)^{-1}, \quad (19)$$

where

$$\Delta_s = \frac{s(2s-1)}{3}. \quad (20)$$

This implies that for large lattice sizes, the energies are (see (18) and (19))

$$E = \frac{3\pi\sqrt{3}}{2L}(\Delta_s + k) + o\left(\frac{1}{L}\right), \quad (21)$$

where  $k$  is an integer. One can observe that the finite-size scaling spectrum of the Hamiltonian is expressed in terms of characters of a Virasoro algebra [13] with a central charge  $c = 0$  (the ground-state has energy zero without finite-size corrections). Hence the system is conformally invariant. This implies a complete knowledge of the finite-size scaling spectrum. In the spin zero sector, for  $L$  even, one gets for the first excitations (see Eqs. (20)-(21)):

$$E_1 = 3\pi\sqrt{3}/L, \quad E_2 = \pi\frac{9\sqrt{3}}{2L}, \dots, \quad (22)$$

which correspond to the values  $\Delta_s = 0$  and  $k = 2, 3, \dots$  in Eq. (21).

In a conformal theory the  $\Delta_s$  given by Eq. (20) are related to the critical exponents of various correlation functions [13]. Notice that

$$\begin{aligned} \Delta_1 &= \frac{1}{3}, \quad \Delta_2 = 2 \quad (L \text{ even}) \\ \Delta_{\frac{3}{2}} &= 1, \quad \Delta_{\frac{5}{2}} = \frac{10}{3} \quad (L \text{ odd}). \end{aligned} \quad (23)$$

Eqs. (22) and (23) will be used in the next sections. The dynamical critical exponent  $z$  of a stochastic process is defined by the finite-size scaling behaviour of the Hamiltonian spectrum:

$$\lim_{L \rightarrow \infty} L^z E = \text{const.} \quad (24)$$

Comparing Eqs. (21) and (24) we conclude that in the RPM,  $z = 1$ .

#### 4. The raise and peel model: combinatorial facets

The TL semigroup algebra (11):

$$e_j^2 = e_j, \quad e_j e_{j \pm 1} e_j = e_j, \quad e_j e_k = e_k e_j \quad \text{for } |j - k| > 1, \quad (25)$$

can be understood in terms of graphs [15]. The generators  $e_j$  can be pictorially represented by

$$e_j = \left[ \begin{array}{c} \cdots \\ \cdots \\ \cdots \\ \cdots \\ \cdots \end{array} \right] \begin{array}{c} \text{---} \\ \text{---} \\ \text{---} \\ \text{---} \\ \text{---} \end{array} \begin{array}{c} \text{---} \\ \text{---} \\ \text{---} \\ \text{---} \\ \text{---} \end{array} \left[ \begin{array}{c} \cdots \\ \cdots \\ \cdots \\ \cdots \\ \cdots \end{array} \right] \quad (26)$$

The words in the left ideal discussed in Section 2 (Eq. (13)) can be represented by boundary diagrams of loops or link patterns [15]. An example of such a diagram is shown in Fig. 1. If the TL semigroup has  $L - 1$  generators one takes  $L$  sites. Contour lines connect pairs of sites and don't intersect.



**Figure 1.** An example of a link pattern for  $L = 16$

The action of  $e_j$  on a link pattern of contour lines is given by placing the graph of  $e_j$  underneath that of the link pattern one, removing the closed loops and the intermediate dashed line. Next, one contracts the links in composite pictures. The action of  $e_1$  on one of the link patterns for  $L = 6$  is given by,

$$(27)$$

We consider the action of the Hamiltonian

$$H = \sum_{j=1}^{L-1} (1 - e_j), \quad (28)$$

on the link patterns. As an example we consider the case  $L = 6$ . In this case we have five words in the ideal  $I_1$ : 1)  $J_0 = e_1 e_3 e_5$ , 2)  $e_2 J_0$ , 3)  $e_4 J_0$ , 4)  $e_2 e_4 J_0$  and 5)  $e_3 e_2 e_4 J_0$ . These words correspond to the link patterns:

1 :		4 :	
2 :		5 :	
3 :			

$$(29)$$

and we find,

$$H = - \begin{pmatrix} -2 & 2 & 2 & 0 & 2 \\ 1 & -3 & 0 & 1 & 0 \\ 1 & 0 & -3 & 1 & 0 \\ 0 & 1 & 1 & -3 & 2 \\ 0 & 0 & 0 & 1 & -4 \end{pmatrix}. \quad (30)$$

Which is indeed an intensity matrix. In the basis (29) the stationary state  $|0\rangle$  of  $H$  is given by

$$|0\rangle = (11, 5, 5, 4, 1). \quad (31)$$

Notice that all the components of  $|0\rangle$  are integer numbers (we have chosen the smallest component to equal 1). The normalization factor  $\langle 0|0\rangle$  (equal to the sum of the components of  $|0\rangle$ ) is equal to 26. Below we show that the normalization factor acquires an extra meaning from an enumeration problem [4]: it is equal to the partition function of an equilibrium statistical mechanics system in two dimensions. This observation has deeper consequences which we will now briefly discuss.

We consider a six-vertex model [30] in a  $(L+1) \times (L+1)$  square lattice with *domain wall boundary condition* [31]. This boundary condition imposes that all the arrows on the vertical (horizontal) boundaries point outward (inward). In Fig. 2(a) we show the fixed links in this boundary condition for the case  $L = 6$ . The arrow configurations on

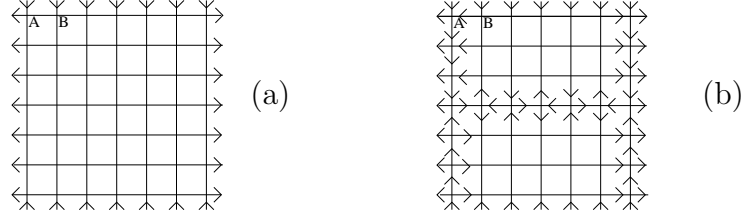


**Figure 2.** a) Domain wall boundary condition for the six-vertex model. b) Fixed arrows for the horizontally symmetric vertex configurations. The lattice size is  $(L+1) \times (L+1)$  with  $L = 6$ .

this lattice can be transformed into FPL configurations. The latter are configurations of paths such that every site is visited by exactly one path. This transformation is done by dividing the square lattice into its even and odd sublattices denoted by A and B, respectively. Instead of arrows, only those edges are drawn that on sublattice A point inward and on sublattice B point outward as in Fig. 3. We take the vertex in the upper left corner to belong to sublattice A.

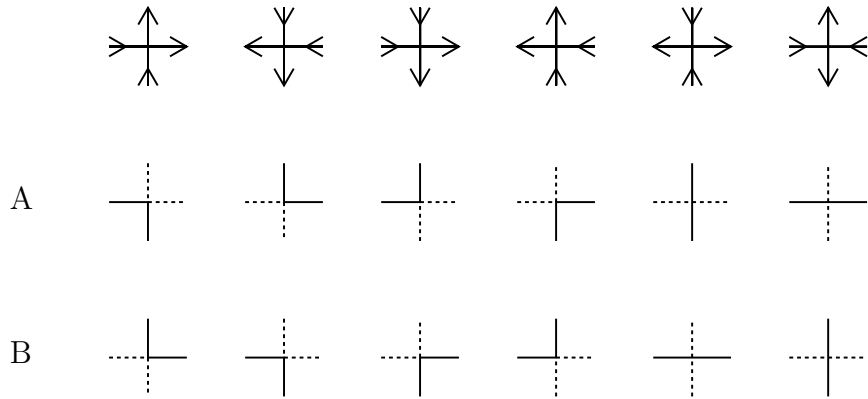


**Figure 3.** FPL vertices on sublattices A and B derived from the six arrow vertices.

The domain wall boundary conditions of the six-vertex model translates into a boundary condition for loops. For example, the boundary condition shown in Fig. 2(a) translates into the boundary conditions given in Fig. 4(a).

Among the general configurations of the vertex model, we now restrict ourselves to those which are horizontally symmetric. In the case of  $L = 6$  the boundary condition is shown in Fig. 2(b). Due to the correspondence of vertices given in Fig. 3 the related FPL configurations will also be horizontally symmetric. In Fig. 4(b) we show the boundary condition for FPL related with that of Fig. 2(b), for  $L = 6$ .

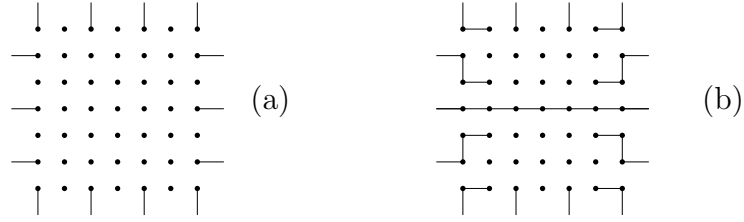


**Figure 4.** a) Boundary conditions (fixed edges) for the FPL diagrams . b) Fixed edges for the horizontally symmetric FPL diagrams. The lattice size is  $(L+1) \times (L+1)$  with  $L = 6$ .

The above relations show that number of horizontally symmetric configurations of the six-vertex model in the  $(L+1) \times (L+1)$  square lattice with domain wall boundary condition is the same as the number of FPL diagrams in the  $(L-1) \times L/2$  rectangular lattice. The boundary condition for the FPL diagrams is special, for the case  $L = 6$  is shown in Fig. 5.

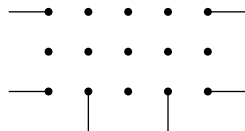


**Figure 5.** FPL grid corresponding to Fig. 2.

The paths that start and end on boundary sites (we disregard the closed loops in the bulk of the FPL diagrams, as a consequence of the correspondence given in Fig. 3) define link patterns having the same topology as the TL link patterns (29). There is a fascinating connection between the components of the stationary state  $|0\rangle$  (see Eq. (31)) and the enumeration of FPL configurations on the rectangular grid: the unnormalized probability of a state corresponding to a given link pattern is equal to the number of FPL configurations with the same link pattern [10, 5]. This is an yet unproven conjecture.

Take for example the stationary state (31) for  $L = 6$ . The FPL configurations on the  $5 \times 3$  rectangle are shown in Fig. 6. Their total number is 26, which is equal to  $\langle 0|0 \rangle$  and they can be categorized according to the five link patterns present in (30). One finds that the number of diagrams corresponding to the link pattern 1 in (29) is 11 (they are printed in bold in Fig. 6), to link pattern 2 is 5, to link pattern 3 is 5, to link pattern 4 is 4 and to link pattern 5 is 1.

We have illustrated for  $L = 6$  the connection between the unnormalized probabilities in the stationary state of various link patterns in the RPM at the Razumov-Stroganov point and the number of FPL configurations with the same link pattern. This connection is important since it shows that one can see a "far from equilibrium" stationary state of an one-dimensional system as an equilibrium state of a system in two dimensions.

Before we further elaborate on this point, we will shortly discuss another facet of the RPM: its connection with the enumeration of alternating sign matrices (ASM) (see

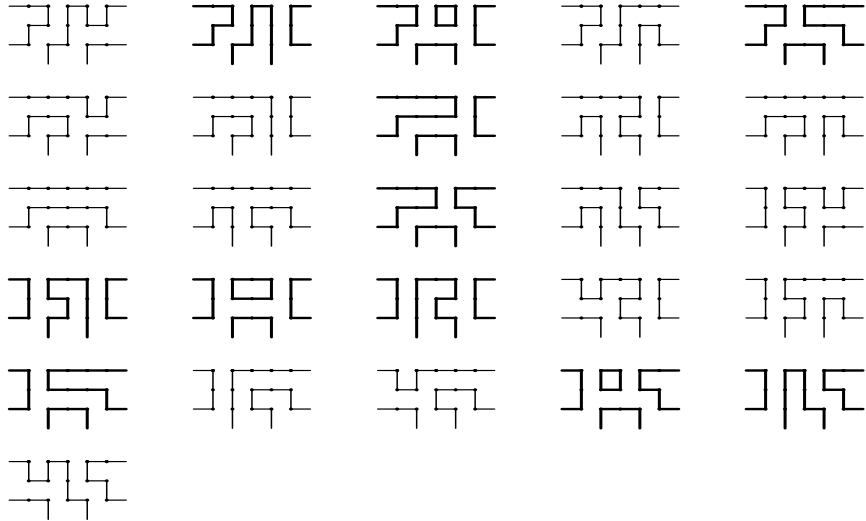


**Figure 6.** The 26 FPL diagrams for  $L = 6$ . The 11 diagrams corresponding to link pattern 1 in (29) are printed in bold.

[9] for an excellent introduction to this subject).

An alternating sign matrix is a square matrix of 0s, 1s and  $-1$ s for which a) the sum of the entries in each row and each column is 1. b) the non-zero entries of each row and of each column alternate in sign. An example of such a matrix is

$$\begin{pmatrix} 0 & 1 & 0 & 0 & 0 \\ 0 & 0 & 1 & 0 & 0 \\ 1 & -1 & 0 & 0 & 1 \\ 0 & 1 & -1 & 1 & 0 \\ 0 & 0 & 1 & 0 & 0 \end{pmatrix}. \quad (32)$$

Alternating sign matrices can have symmetry properties. For example, the matrix

$$\begin{pmatrix} 0 & 1 & 0 \\ 1 & -1 & 1 \\ 0 & 1 & 0 \end{pmatrix} \quad (33)$$

is vertically and horizontally symmetric. There is a one to one correspondence between the six-vertex configurations with domain-wall boundary conditions and ASM. To each vertex you attach the numbers 0,  $-1$  or 1 as shown in Fig. 7. To six-vertex configurations with a certain symmetry correspond alternating sign matrices with the same symmetry.

The number of six-vertex configurations on a  $(L+1) \times (L+1)$  square with domain wall boundary conditions that are invariant under reflection in the horizontal symmetry axis is equal to that of the  $(L-1) \times L/2$  rectangle with special boundary conditions like in Fig. 2(b). The total number of such configurations is known and is equal to the number of  $(L+1) \times (L+1)$  horizontally symmetric ASM (equal to the number of

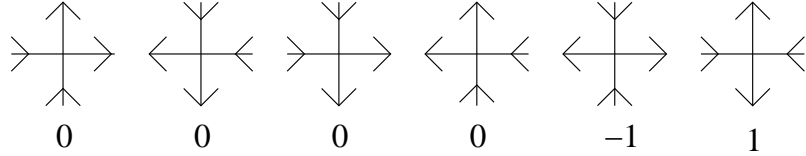


**Figure 7.** Correspondence between vertices and entries of alternating sign matrices.

vertically symmetric ASM) which is given by [32]:

$$A_{2n+1}^V = \prod_{j=0}^{n-1} (3j+2) \frac{(2j+1)!(6j+3)!}{(4j+2)!(4j+3)!} = 1, 3, 26, 646, \dots, \quad (34)$$

where  $L = 2n$ . The leading asymptotic terms of  $A_{L+1}^V$  are given by

$$\ln A_{L+1}^V = s_0 \frac{(L-1)L}{2} + (L-1) \ln \frac{3\sqrt{6}}{8} - \frac{5}{144} \ln L^2 + O(1), \quad (35)$$

where  $s_0 = \ln(\frac{3\sqrt{3}}{4})$ . The first term is proportional to the area of the rectangle, the second one is related to the boundary. This shows that, indeed, the stationary state of the RPM is related to a *bona fide* two-dimensional statistical mechanics system.

In the next section we are going to discuss physical applications of the stochastic model defined by the Hamiltonian  $H$  (Eq. (28)) acting on the vector space of link patterns (see, for  $L = 6$ , Eq. (29)). In the Appendix we show how each link pattern can be mapped onto a RSOS (Dick) path. Such a path can be seen as an one-dimensional interface separating clusters of "tiles" deposited on a substrate, from a rarefied gas of tiles. The action of the Hamiltonian  $H$  on the RSOS configurations gives the transition rates for various adsorption and desorption processes (see Eqs. (29), (30) and Fig. A2 for an example with  $L = 6$ ).

## 5. The raise and peel model: the phase diagram

We consider a one-dimensional lattice with  $L+1$  ( $L = 2n$ ) sites. An interface is formed by attaching at each site non-negative integer heights  $h_i$  ( $i = 0, 1, \dots, L$ ) which obey the restricted solid-on-solid (RSOS) rules:

$$h_{i+1} - h_i = \pm 1, \quad h_0 = h_L = 0, \quad h_i \geq 0. \quad (36)$$

There are  $C_n = (2n)!/((n+1)(n!)^2)$  possible configurations of the interface, that also correspond to the number of independent words (14) in the left ideal  $I_1$  given in (13) (see Sec. 4). In Fig. 1 we show a configuration for  $n = 8$  ( $L = 16$ ). Alternatively, one can describe the interface using slope variables  $s_i = (h_{i+1} - h_{i-1})/2$ , ( $i = 1, \dots, L-1$ ).

The dynamics of the interface is described in a transparent way in the language of tiles (tilted squares) which cover the area between the interface and the substrate ( $h_{2i} = 0$ ,  $h_{2i+1} = 1$ , ( $i = 0, \dots, n-1$ ),  $h_L = 0$ ) (see Fig. 8).

We consider the interface separating a film of tiles deposited on the substrate from a rarefied gas of tiles. The evolution of the system in discrete time (Monte-Carlo steps)

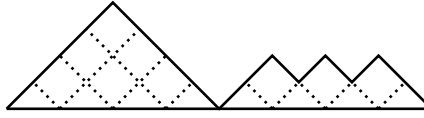


**Figure 8.** A configuration of the interface with three contact points and two clusters, as defined in Sec. 6, for the lattice size  $L = 16$ .

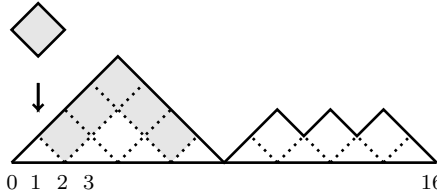


**Figure 9.** A desorption event. The incoming tile at site 1 triggers, with probability  $u_d$ , an avalanche of 5 tiles, which are shaded. All of the shaded tiles are removed in the desorption event.

is given by the following rules. With a probability  $P_i = 1/(L-1)$  a tile from the gas hits site  $i$ , ( $i = 1, \dots, L-1$ ). Depending on the value of the slope  $s_i$  at the site  $i$ , the following processes can occur:

- i)  $s_i = 0$  and  $h_i > h_{i-1}$ .  
The tile hits a local peak and is reflected.
- ii)  $s_i = 0$  and  $h_i < h_{i-1}$ .  
The tile hits a local minimum. With a probability  $u_a$  the tile is adsorbed ( $h_i \mapsto h_i + 2$ ) and with a probability  $1 - u_a$  the tile is reflected.
- iii)  $s_i = 1$ .  
With probability  $u_d$  the tile is reflected after triggering the desorption of a layer of tiles from the segment ( $h_j > h_i = h_{i+b}$ ,  $j = i+1, \dots, i+b-1$ ), *i.e.*  $h_j \mapsto h_j - 2$  for  $j = i+1, \dots, i+b-1$ . This layer contains  $b-1$  tiles (this is always an odd number). With a probability  $1 - u_d$ , the tile is reflected and no desorption takes place. For an example see Fig. 9.
- iv)  $s_i = -1$ .  
With probability  $u_d$  the tile is reflected after triggering the desorption of a layer of tiles belonging to the segment ( $h_j > h_i = h_{i-b}$ ,  $j = i-b+1, \dots, i-1$ ), *i.e.*  $h_j \mapsto h_j - 2$  for  $j = i-b+1, \dots, i-1$ . With a probability  $1 - u_d$  the tile is reflected and no desorption takes place.

The physics of the model depends on one parameter  $u = 1/w = u_a/u_d$ . We use these notations since we consider below either very small values of  $w$  (or  $u$ ) and our intuition can be helped by the fact that for  $u = 0$  or  $w = 0$  the properties of the system are known. Namely, for both  $u = 0$  and  $w = 0$  the spectrum is massive [1], the stationary states being the substrate ( $u = 0$ ) and a full triangle ( $w = 0$ ), *i. e.*,  $h_i = h_{L-i}$  ( $i = 1, \dots, L/2$ ).

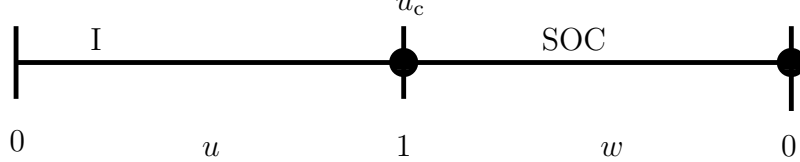


**Figure 10.** Phase diagram of the raise and peel model. For  $0 \leq u < 1$  (phase I), the model is massive. At  $u = u_c = 1$  it is massless and conformal invariant. For  $1 > w > 0$  it is scale invariant with varying critical exponents and exhibits SOC. For  $w = 0$  the system is massive.

At the special point of the RPM where the ratio  $u = u_a/u_d = 1/w = 1$  (the Razumov-Stroganov point considered in earlier sections) the model is governed by the Temperley-Lieb Hamiltonian (28) acting on the space of configurations by the ideal  $I_1$  defined in (13) (see Sec. 4 and Appendix). As a consequence, the model is exactly integrable and conformally invariant. As discussed in Sec. 3 this last invariance allows exact predictions for the finite-size eigenspectrum of  $H$ . For  $u \neq 1$  the model is not exact integrable anymore and our knowledge comes from Monte Carlo simulations [2].

The phase diagram of the model obtained from the Monte Carlo simulations is given in Fig. 10. In the domain  $0 < u < 1$  the system is massive undergoing a second order phase transition at  $u = u_c = 1$ . For  $1 > w > 0$  the conformal symmetry seen at  $w = 1$  is broken but the system stays scale invariant. Since in this domain one has avalanches we call this phase a self-organized criticality (SOC) phase. Another phase transition occurs at  $w = 0$  where the system becomes massive again. The phase diagram of Fig. 10 was established from the static and dynamic properties of the RPM [2]. In the next section we are going to consider the static properties of the stationary state and in Section 7 the dynamical ones.

## 6. The stationary state of the RPM

It is useful to define some quantities which characterize the surface. An obvious geometric observable is the set of sites  $j$  ( $j$  even) for which  $h_j = 0$  (the sites 0 and  $L$  always belong to this set). These sites are also called contact points. This set is important, for example, to study desorption. Desorption events are limited to the area between two contact points, defined as a cluster (see Fig. 8). The density of contact points gives a local observable for which one can define various correlation functions.

We first define quantities in the stationary state. The average number of clusters  $k(L)$ , the density of clusters  $\rho(L)$  and the local density of clusters  $g(j, L)$  are defined by:

$$k(L) = \sum_{j=1}^L g(j, L) = \left\langle \sum_{j=1}^L \delta_{h_j, 0} \right\rangle, \quad (37)$$

$$\rho(L) = k(L)/L. \quad (38)$$

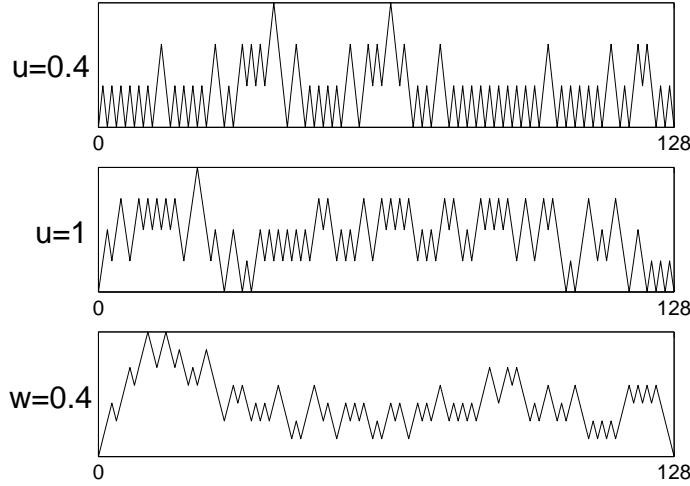


**Figure 11.** Typical configurations in the stationary states for  $L = 128$  sites and three values of  $u$ .

Note that the maximum value of  $\rho(L)$  is  $\frac{1}{2}$  which is obtained when  $u = 0$  and one has only one configuration in the system: the substrate. The average height is defined as:

$$h(L) = \frac{\langle \sum_{j=1}^L h_j \rangle}{L}. \quad (39)$$

The lowest value of  $h(L)$ , corresponding to the substrate, is  $\frac{1}{2}$ . It is useful to consider also the average height in the middle of the system:

$$h_{\frac{1}{2}}(L) = \langle h_{\frac{L}{2}} \rangle. \quad (40)$$

A relevant quantity is the average of the fraction of the interface where desorption does not take place (FND)

$$n(L) = \frac{1}{L-1} \langle \sum_{j=1}^{L-1} (1 - |s_j|) \rangle. \quad (41)$$

This quantity allows to estimate the average number of tiles desorbed in avalanches (see Sec. 7). By studying the behaviour of  $n(L)$  for large  $L$  and various values of  $w$  we will be able to establish the existence of a discontinuous phase transition at  $w = 0$ .

The large  $L$  behavior of any of the quantities (37)-(41), say  $h(L)$ , will be denoted  $h_\infty$ :

$$h_\infty \equiv \lim_{L \rightarrow \infty} h(L). \quad (42)$$

In the next section we are going to discuss average quantities which are not only  $L$  dependent but also time dependent. For these quantities we use, for example, the notation  $k(t, L)$  to denote the number of clusters.

In order to get an intuition on the behavior of the model when  $u$  (or  $w = 1/u$ ) changes, in Fig. 11 we show, for  $L = 128$ , typical configurations in the stationary states for three values of the parameter  $u$ . One notices that for  $u = 0.4$  there are many clusters,

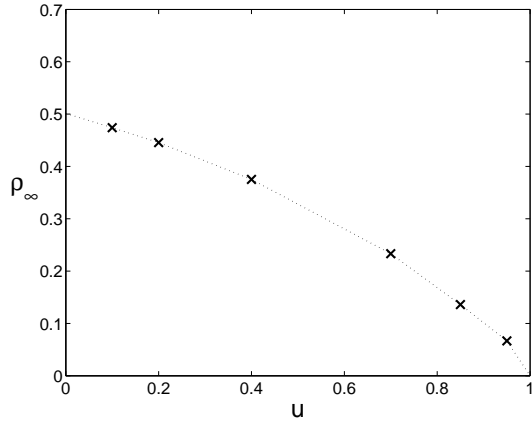


**Figure 12.** The density of clusters  $\rho_\infty$  for various values of  $u < 1$ .

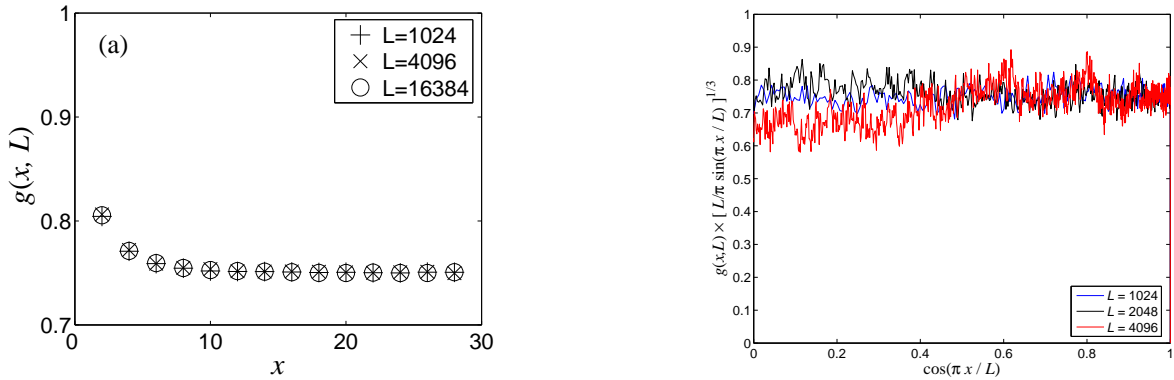


**Figure 13.** (a) The local density of contact points  $g(x, L)$  at  $u = 0.4$  for different lattice sizes  $L$  ( $g(x, L)$  is zero for  $x$  even). (b) (Color online) The scaling function  $C(\cos(\pi x/L))$  defined in (46) for  $u = 1$ .

fewer for  $u = 1$  and a single one for  $w = 0.4$  (other, less probable, configurations do exhibit several clusters). We also notice that the average heights are quite small.

We first consider the density of clusters  $\rho(L)$  in the domain  $0 \leq u < 1$ . Taking large values of  $L$ , one obtains the  $u$  dependence of  $\rho_\infty$  shown in Fig. 12. In all this domain the density of clusters stays finite. The density of clusters decreases from its maximum possible value  $1/2$  which corresponds to the substrate at  $u = 0$  to the value zero for  $u = 1$ . This indicates that there is a phase transition at  $u = 1$ . From the Monte Carlo simulations it was hard to obtain the critical exponent which gives  $\rho(u)$  when  $u$  approaches the value one.

The local density of contact points  $g(x, L)$  (see Eq. (37)) for  $u = 0.4$  and different lattice sizes is shown in Fig. 13(a). One observes that for small values of  $x$ , and large values of  $L$ ,  $g(x, L)$  decreases exponentially from the value 1 at  $x = 0$  (not shown on Fig. 13(a)) to a constant value in the bulk. This value is twice that seen in Fig. 12, since for even  $x$  one always have  $g(x) = 0$ .

Since for  $u = 0$  one can diagonalize the related Hamiltonian of the stochastic process

and show rigorously [1] that the system is massive, we can expect that the system is massive in the whole domain  $0 \leq u < 1$ .

We turn now to the interesting case  $u = 1$  where the system is exact integrable and conformally invariant. In Ref. [8] a conjecture was made which gives the probability  $P_n(k)$  to have  $k$  clusters in a system of size  $L = 2n$ :

$$P_n(k) = k \frac{4^{n+k}}{27^n} \frac{\Gamma(\frac{1}{2} + n + k) \Gamma(\frac{1}{3}) \Gamma(3n + 2) \Gamma(2n - k)}{\Gamma(\frac{1}{2}) \Gamma(\frac{1}{3} + 2n + k) \Gamma(n + 1) \Gamma(2n + k + 2) \Gamma(n - k + 1)}. \quad (43)$$

The last result gives us the leading behaviour

$$k(L) = \sum_{k=1}^n k P_n(k) \simeq \frac{\Gamma(1/3) \sqrt{3}}{2\pi} L^{\frac{2}{3}}, \quad (44)$$

for the average number of clusters. This shows that the density of clusters vanishes algebraically for  $u = 1$ . This conjecture was checked using Monte Carlo simulations up to a system of size  $L = 512$ . Since, as we show below, the density of clusters also vanishes algebraically in the entire domain  $u < 1$ , it is convenient to define a critical exponent  $\alpha < 1$  which gives the power law increase of the number of clusters with the system size,  $k(L) \sim L^\alpha$ . For  $u = 1$  we have obviously  $\alpha = 2/3$ .

It is interesting to consider, again for  $u = 1$ , the density of contact points  $g(x, L)$  for several lattice sizes and notice that for the function

$$G(x/L) = L^{\frac{1}{3}} g(x, L), \quad (45)$$

one has a data collapse. As suggested by the conformal invariance for the confined critical systems [33] we make an *ansatz* about the functional behaviour of  $G(x/L)$  taking:

$$g(x, L) = \left[ \frac{L}{\pi} \sin(\pi x/L) \right]^{-1/3} C(\cos(\pi x/L)). \quad (46)$$

In Fig. 13(b) one shows the function  $C(\cos(\pi x/L))$ . It is practically a constant. If one assume that  $C$  is independent of  $\pi x/L$ , one can get its value by integrating  $g(x, L)$  (Eq. (46)) and compare the result with the average number of clusters given by (44). One obtains:

$$C = -\frac{\sqrt{3}}{6\pi^{\frac{5}{6}}} \Gamma\left(-\frac{1}{6}\right) = 0.753149..., \quad (47)$$

in very good agreement with the data obtained from Monte Carlo simulations (see Fig. 13(b)).

The motivations for the *ansatz* (46) comes from the following observation. If the density of contact points corresponds to a local operator in conformal field theory, one expects [33],

$$g(x, L) = C \left[ \frac{L}{\pi} \sin(\pi x/L) \right]^X, \quad (48)$$

where  $X = \Delta + \bar{\Delta}$  is the scaling dimension of the local operator ( $\Delta - \bar{\Delta}$  is the conformal spin). Comparing Eqs. (46)-(48) one concludes that the density of contact points corresponds to a local operator with scaling dimensions  $X = 1/3$ . This result is surprising. One can show that the profile of an operator with spin vanishes [33].

w	1	0.85	0.75	0.4	0.25	0.1	0.05	0.025
$\alpha$	0.67	0.50	0.40	0.30	0.24	0.15	0.06	0.01

**Table 1.** Estimates of the exponent  $\alpha$  giving the increase of the number of clusters with the size of the system  $L$ . These data were obtained from numerical analysed of several lattice sizes up to  $L = 65536$ .

This implies  $\Delta = \bar{\Delta} = 1/6$ . This value can't be obtained from the possible values of  $\Delta$  (see (20)) of minimal models. It might be obtained from  $W(A_n)$  algebras [34, 35] but it is not clear why W-symmetry should play any role in our problem. Another possible explanation is that for a conformal theory with  $c = 0$  (this is also the case of percolation), under certain circumstances, the scaling dimension can be an arbitrary number [36, 37]. This possibility is a bit strange since the number one has to obtain is a neat  $1/6$ . Finally, it is possible, that the proof that operators with spin have no profile functions does not apply to our problem. If this is the case, one can choose  $\bar{\Delta} = 0$  and  $\Delta = 1/3$  §. The value  $1/3$  is a perfectly acceptable one (see Eq. (23) in Sec. 3). To conclude, we have not yet an explanation for the value  $X = 1/3$  in Eq. (48).

We move away from  $u = 1$  and consider the domain  $1 > w$ . The number of clusters  $k(L)$  keep having an algebraic increase with an exponent  $\alpha$  that decreases monotonically with  $w$ . In Table 1 we give estimates for the exponent  $\alpha$  for several values of  $w$ . It was also observed that for several values of  $w$  the scaling law

$$G(x/L) = L^{1-\alpha} g(x, L) \quad (49)$$

holds.

These results indicate that for  $u > 1$  the system stays scale invariant with a varying critical exponent.

Although it seems obvious that one should look at the  $L$  dependence of the average value of the heights  $h(L)$  or the average value of the height at the middle of the lattice  $h_{\frac{1}{2}}(L)$ , it turns out that these quantities are harder to study since they vary slowly with the system size (see [2] for some illustrating figures). In the case of  $h_{\frac{1}{2}}(L)$  we have the dependence shown in Fig. 14(a).

A different picture emerges if one considers very small values of  $w$  as shown in Fig. 14(b). One can observe two different phenomena. The values of  $h_{\frac{1}{2}}(L)$  increase substantially as compared to the values observed at larger values of  $w$ , and more interestingly, it looks like they saturate for large values of  $L$ . We believe [2] that this saturation phenomena happens in the whole region  $u > 1$  ( $w < 1$ ). We did not see such saturation for smaller values of  $u$  (see Fig. 14(a)) because the lattice sizes considered in the simulations was not large enough for these values of  $u$ . Considering these simulations with lattice size  $L = 65536$  a good fit, for various values of  $w$ , is obtained by the curve

§ For the appearance of operators with conformal spin in the presence of the quantum group symmetry mentioned in Sec. 3, see Ref. [38].

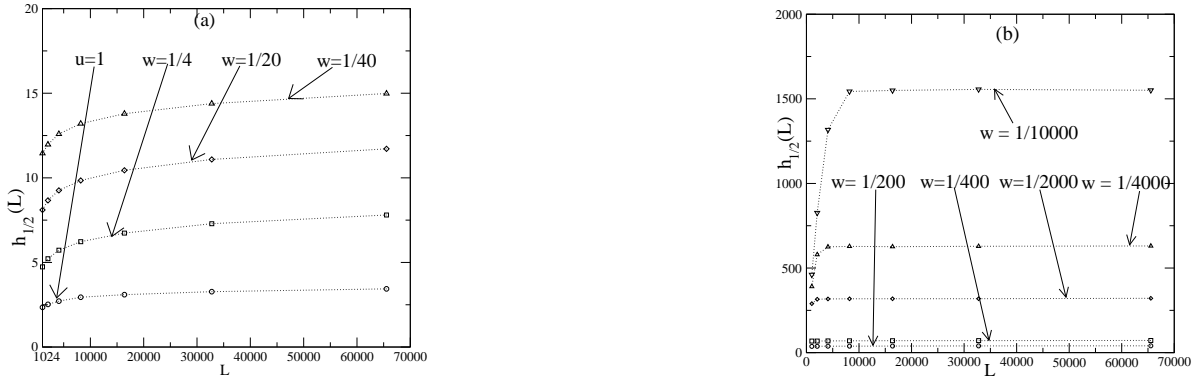


**Figure 14.** (a) Average height in the middle of the lattice  $h_{1/2}(L)$  as a function of the lattice size  $L$  for some values of  $w$  in the range  $1 \geq w \geq 0.025$ . (b) Average height in the middle of the lattice  $h_{1/2}(L)$  as a function of the lattice size  $L$  for various small values of  $w$  ( $w \leq 1/200$ ).

[2]

$$h_{\max} = \frac{4.67}{w^{0.62}}. \quad (50)$$

Interestingly, if we use (50) for  $w = 1$  we obtain  $h_{\max} = 4.67$ , a value compatible with the results shown in Fig. 14(a). Taking the results shown in Fig. 14(b) at face value, implies that the phase SOC (see Fig. 10) extends at least to the value  $w = 10^{-4}$ . On the other hand for  $w = 0$  the single configuration is the full triangle,  $h_{\max}$  has values of the size of the system and therefore the  $L$ -dependence of  $h_{\max}$  shows no saturation. This suggests a non-analytical behaviour of various quantities describing the system at  $w = 0$ . In order to illustrate this point, in Fig. 15 we show typical configurations in the stationary state for a very small value of  $w$  ( $w = 0.00025$ ) and different system sizes. One can see a clear change in the role of the boundaries if  $L$  varies from 1024 to 32768. For  $L = 1024$  one is close to the full triangle configuration (expected for  $w = 0$ ). However, as one increases  $L$ , one gets a plateau (in which the height is almost constant and  $L$  independent) and the boundaries play a less and less important role.

## 7. Space-time phenomena and avalanches

In the last section we present results that corroborate the phase diagram shown in Fig. 10. In the present section we give additional facts supporting these results. We are going to use the Family-Vicsek [39] scaling in order to check if the system is in a scale invariant phase and if the answer is positive, determine the dynamical critical exponent  $z$ . If we consider a time-dependent average quantity  $a(t, L)$ , being  $a(L)$  the average in the stationary state, than for large values of  $t$  and  $L$  the function  $A(t, L)$  scales as:

$$A(t, L) = \frac{a(t, L)}{a(L)} - 1 \sim A\left(\frac{t}{L^z}\right), \quad (51)$$

where  $z$  is the dynamical critical exponent. The scaling function depends on the initial conditions. In the data shown below, we have taken as initial condition the substrate

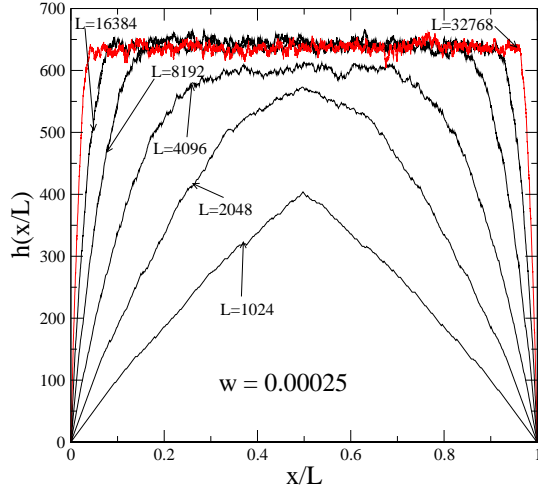


**Figure 15.** (Color online) Typical configurations in the stationary state for  $w = 0.00025$  and different values of  $L$ .

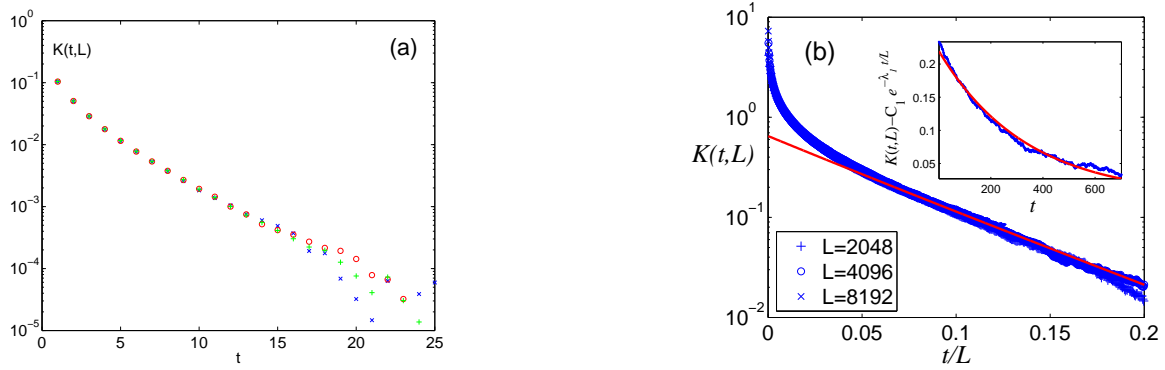


**Figure 16.** (Color online) (a) Function  $K(t, L)$ , defined on (51), for  $u = 0.4$  as a function of time for the lattice sizes  $L = 2048, 4096$  and  $8192$ . (b) Function  $K(t, L)$  for  $u = 1$  as a function of  $t/L$  for various lattice sizes. Red curve is given by a fit to (51) considering only the first exponential with  $\lambda_1 = \pi 3\sqrt{3}$  and  $C_1 = 0.18$ . In the inset we compare  $K(t, L) - C_1 e^{-\lambda_1 t/L}$  for  $L = 8192$  with the short time exponential  $C_2 e^{-\lambda_2 t/L}$ , given in red line (color online) with  $\lambda_2 = \frac{3}{2}\lambda_1$  and  $C_2 = 0.54$ .

$(h(2i) = 0, h(2i + 1) = 1, (i = 0, \dots, n - 1), h_L = 0)$  with probability one. We first consider the quantity  $K(t, L)$  which corresponds to the average number of clusters ( $a(t, L)$  in (51) is  $k(t, L)$  in this case).

In Fig. 16(a) we show the function  $K(t, L)$  for  $u = 0.4$  for different lattice sizes. We notice that for large lattice sizes,  $K(t, L)$  is a function on  $t$  only and can be obviously fitted with a sum of exponential functions as expected in a massive phase. Fig. 16(b) shows  $K(t, L)$  for  $u = 1$  and as expected from conformal invariance,  $z = 1$ . Conformal invariance gives also information on the function  $K(t, L)$ . One can use the knowledge of the finite-size scaling limit spectrum and obtain the functional dependence of  $K(t/L)$ . To illustrate how it works see Fig. 16(b). For large values of  $t/L$  one can do a fit to the

$w$	$K$	$H$	$H_{1/2}$
1	1.03	0.95	0.97
0.9	0.86	0.74	0.72
0.7	0.55	0.52	0.50
0.4	0.35	0.34	0.34
0.25	0.31	0.30	0.30
0.025	*	0.07	0.07

**Table 2.** Estimates of the dynamical critical exponent  $z$  for various values of  $w$ . The estimates were obtained using (51) with  $A$  replaced by  $K$ ,  $H$  and  $H_{\frac{1}{2}}$ . The number represented by (\*) is not reliable since in that region the number of clusters is very small. These estimates were obtained by considering several lattice sizes up to  $L = 65536$ .

data, using the following ansatz:

$$K(t/L) = C_1 e^{-\frac{\lambda_1 t}{L}} + C_2 e^{-\frac{\lambda_2 t}{L}}, \quad (52)$$

where the  $\lambda_i$  are obtained from the spectrum of the Hamiltonian (28), given by (22):

$$E_i = \frac{\lambda_i}{L}, \quad i = 1, 2. \quad (53)$$

The constants  $C_i$  depend on the initial conditions. If one starts with the substrate  $C_1 = 0.28$  and  $C_2 = 0.54$ .

We now consider smaller values of  $w$  (larger values of  $u$ ). We have done an extensive study of various functions  $A(t, L)$  taking  $K(t, L)$ ,  $H(t, L)$  and  $H_{\frac{1}{2}}(t, L)$  in (51). The estimated values for the critical exponent  $z$  are shown in Table 2. For very small values of  $w$ , the estimates coming from  $K(t, L)$  are poor because the number of clusters is small and hence large errors. Inspection of table 2 shows a smooth drop of the values of  $z$  from  $z = 1$  for  $w = 1$  to  $z \approx 0$  for  $w \approx 0$ . The latter values is in agreement with a direct calculation of the mass gap at  $w = 0$  [1] which gives a finite gap in the thermodynamic limit. In the region where  $z \rightarrow 0$  the information propagates, through the system, at infinite velocity. This can be explained nicely by Fig. 15 for large  $L$ . If the dynamics chooses a site near the edges, the peel process affects almost the whole interface, simultaneously lowering the entire upper plateau by a unit, implying that the information travelled an infinitely long distance in the limit  $L \rightarrow \infty$  [40].

We have not studied extensively the two-contact points space-time correlation functions  $c(R, t, L)$ , except for the special case  $u = 1$ . This case is interesting since from conformal invariance it exhibits, far from the boundaries, the following scaling form in the bulk (see (45)):

$$C(R, t, L) = L^{-\frac{2}{3}} G(\mu), \quad (54)$$

where

$$\mu = \frac{\sqrt{R^2 + v_s^2 t^2}}{L}. \quad (55)$$

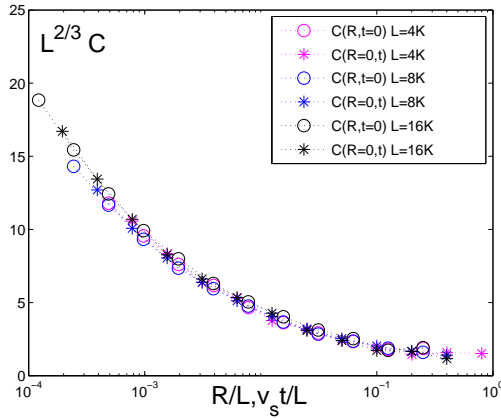


**Figure 17.** (Color online) The two-contact point correlation function  $C(R, t, L)$  times  $L^{\frac{2}{3}}$  as a function of the scaled distance  $R/L$  and the scaled time  $\frac{v_s}{L}t$  ( $v_s = \frac{3}{2}\sqrt{3}$  is the sound velocity) for various lattice sizes.

In (54) and (55)  $R$  is the distance between the contact points,  $t$  is the time difference and  $v_s = \frac{3}{2}\sqrt{3}$  is the sound velocity [2]. The factor  $L^{-\frac{2}{3}}$  in (54) is obtained from (45). In Fig. 17 we show the scaling function  $G(\mu)$ , where we have used the unconnected correlation function in (54). To avoid boundary effects the data was taken only in the center segment of size  $L/2$ .

The functional dependence (54) which is special for the conformal invariant case is nicely seen in Fig. 17. Our data are not good enough in order to extract from the small  $\mu$  behavior of  $G(\mu)$ , the two-contact point correlation function in the thermodynamic limit.

An interesting property of the RPM is the occurrence of avalanches in the desorption processes. For the case  $u = 1$ , based on exact results on small lattices, the existence of avalanches was suggested in [1]. The Monte Carlo simulations on large lattices show avalanches in the whole domain  $0 < w \leq 1$ .

In the stationary state, once a tile from the rarefied gas hits the interface, it can be reflected, adsorbed or can trigger a nonlocal desorption process in which many tiles may leave the interface, this defines an avalanche. In the latter case the size of the avalanche is given by the number of tiles  $T$  that are released in the process. This number is always odd, therefore it is convenient to write:  $T = 2v - 1$  ( $v = 1, 2, \dots$ ). For  $u < 1$  only a finite number of tiles are removed, since the density of clusters is finite. For  $w \leq 1$ , the cluster density vanishes, and therefore macroscopic number of tiles may be desorbed, hence macroscopic avalanches.

We denote by  $S(v, L)$  the PDF which gives the probability for an avalanche of size  $v$  for a system of size  $L$ . In models of self-organized criticality (SOC) [41]-[45], for large values of  $v$  and  $L$ , one may expect the PDF to exhibit a simple scaling law,

$$S(v, L) = v^{-\tau} F\left(\frac{v}{L^D}\right), \quad (56)$$

characterized by two exponents  $\tau$  and  $D$ .

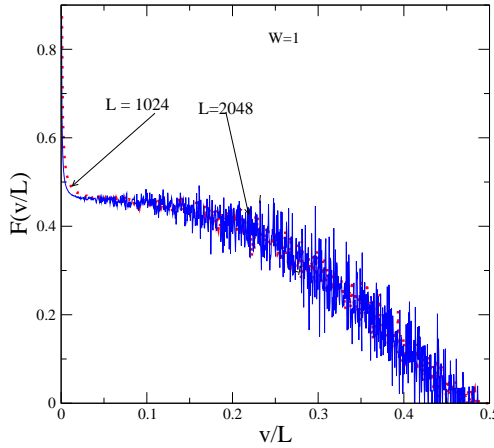


**Figure 18.** (Color online) The scaling function  $F(v/L)$  for  $w = 1$ . The data are for lattice sizes  $L = 1024$  and  $L = 2048$ .

$w$	1	0.95	0.90	0.80	0.60	0.45	0.30	0.05	0.02	0.005
$D$	1.004	1.089	1.087	1.066	1.040	1.026	1.017	1.002	1.002	1.006
$\tau$	3.00	2.77	2.63	2.47	2.32	2.25	2.18	2.07	2.046	2.00

**Table 3.** Estimates of the critical exponents  $D$  and  $\tau$  obtained by using lattices sizes  $L = 4096$  and  $L' = 8196$ .

The Monte Carlo simulations [2] allow the evaluation of the above exponents. For  $u = 1$  we have  $\tau \approx 3$  and  $D \approx 1$ . The result  $D = 1$  is to be expected since in a conformal invariant theory (this is the case if  $u = 1$ ) one has no other length than the size of the system  $L$ . We found no explanation for the value three of  $\tau$  although this number shows up in many aspects of the model (see for example (45)). In Fig. 18 we show the scaling function  $F(v/L)$  defined in (56). One observe a nice data collapse.

In Table 3 we give the estimates for the exponent  $D$  and  $\tau$  for various values of  $w$ . The estimates presented in this Table are obtained using only one pair of sizes (4096 and 8192) but we made sure that the results are reliable by studying the changes of the values of the estimates using smaller lattices.

The results of Table 3 indicate that the exponent  $D$  stays unchanged and equals to one in the whole range  $w < 1$ . This can be understood in the following way [46] the tiles which are desorbed and create the avalanche belong always to a one-dimensional layer.

We turn now to the exponent  $\tau$ . As can be seen in Table 3 this exponent varies from the value 3 ( $u = 1$ ) to a value close to 2 for  $w$  close to zero. In the case  $u = 1$ , the average size of the avalanches stays finite when  $L$  gets large but the dispersion diverges (the function  $F(v/L)$  shown in Fig. 18 does not vanish at the origin). Does an exponent  $\tau = 2$  mean that the average size of the avalanches diverges logarithmically with  $L$ ? Not necessarily, it depends if the scaling function  $F(v/L)$  vanishes or not at the origin. In Fig. 19 we show for  $w = 0.00025$ , that  $F(v/L)$  does not vanish at the origin. Since later in this section we are going to show that  $\langle v \rangle$  stays finite for any  $w > 0$ , we conclude that

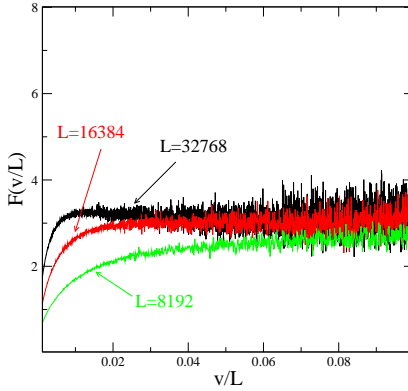


**Figure 19.** (Color online) The functions  $F(v/L)$ , defined on (56), at  $w = 0.00025$  for some values of  $L$ .

$\tau$  gets very close to the value 2 but never reaches it. For a more precise determination of the exponent  $\tau$ , see Figs. 15-18 in Ref. [2].

The Monte Carlo simulations show avalanches at least in the interval  $1 \geq w \geq 0.00025$  and therefore the system is scale invariant in this interval. It is probably safe to assume that the SOC phase covers the domain  $1 \geq w > 0$ . It was checked that for  $u < 1$ , where the system is massive, for large values of  $v$  the PDF has an exponential decrease and not an algebraic one.

We turn now our attention to the average size of the avalanches. A simple mean-field argument allows to compute it using informations about the stationary state only.

We first consider, in the stationary state, the average fraction of interface where desorption does not take place  $n(L)$  (FND) defined in (41). This quantity varies from the value 1 for the substrate (the single configuration for  $u = 0$ ) to the value  $1/(L - 1)$  for the full triangle (the single configuration for  $w = 0$ ).

For  $u = 1$  there is a conjecture [47] for the values of  $n(L)$

$$n(L) = \frac{3L^2 - 2L + 2}{(L - 1)(4L + 2)} = \frac{3}{4}\left(1 - \frac{1}{6L} + \dots\right). \quad (57)$$

This conjecture was checked using our Monte Carlo simulations for various lattice sizes.

If one knows  $n(L)$ , the average probability  $P_a(L)$  to have an adsorption process, the average probability  $P_r(L)$  to have a reflection process and the average probability  $P_d(L)$  to have a desorption process can be easily obtained:

$$P_a(L) = \frac{n(L)}{2} - \frac{1}{2(L - 1)}, \quad (58)$$

$$P_r(L) = \frac{n(L)}{2}(2w - 1) + 1 - w + \frac{1}{2(L - 1)}, \quad (59)$$

$$P_a(L) + P_r(L) + P_d(L) = 1, \quad (60)$$

where we choose  $u_a = 1$  and  $u_d = w = 1/u$ .

Taking into account that in the stationary state the average number of adsorbed tiles is equal to the average number of desorbed tiles, one obtains:

$$\langle T \rangle_L = 2\langle v \rangle_L - 1 = \frac{P_a(L)}{P_d(L)}. \quad (61)$$

Note that this is a mean-field calculation since we have first computed the average probability to have a desorption process and multiplied it with the average number of tiles which are desorbed. In the large  $L$  limit (58)-(61) gives:

$$\langle T \rangle_\infty \approx \frac{n_\infty}{2(1 - n_\infty)w}. \quad (62)$$

In Fig. 20 one shows the  $w$  dependence of  $n_\infty$  as obtained from the extrapolated results of our Monte Carlo simulations. One notices a discontinuous behavior of  $n_\infty$  around  $w = 0$ . At  $w = 0$  where in the stationary state one has only one configuration, which is the full triangle (see Fig. A2), one has  $n_\infty = 0$ , while  $\lim_{w \rightarrow 0^+} n_\infty = 0.5$ . Using (62) one concludes, in agreement with previous observations, that for any finite value  $w$ , the average size of the avalanches is finite. We consider that the discontinuity of  $n_\infty$  at  $w = 0$  shown in Fig. 20 is one of the most interesting and unexpected property of the model. The value  $n_\infty = 0.5$  observed for  $w = 0^+$  corresponds to an interface in which on the average we have an equal number of sites where one has local minima, maxima, positive or negative slopes. It is not clear to us why this interface is special. The existence of this discontinuity also gives supplementary support for the existence of the SOC phase. Studying the finite-size scaling properties of the Hamiltonian spectra for small lattices and different values of  $w$  in Ref. [1] it was shown that for  $w < 1$  one does not have conformal invariance. On the other hand, for  $w = 0$ , we know [1] that the system has an energy gap. In spite of all our determinations of critical exponents in the domain  $0 < w < 1$  implying that the system is gapless, one could argue that one sees crossover effects and that one can have a massive phase in the whole domain  $0 \leq w < 1$ . The discontinuity observed in the behaviour of  $n_\infty$  assures us that this is not the case.

In Table 4 we compare in two cases the mean-field predictions for  $\langle T \rangle_L$  given in (62) with the values measured in Monte-Carlo simulations. The agreement is excellent. In the same Table the values for  $n(L)$  for several values of  $L$  are also given. One notices that for  $w = 1$  and  $L = 1024$  one already gets, within five digits, the asymptotic value  $3/4$ . This is not the case for  $w = 0.00025$ , where the finite-size effects are larger. Our numerical analysis indicate that the asymptotic behavior of  $n(L)$  can be described by

$$n(L) = n_\infty(1 - A(w)/L + \dots), \quad (63)$$

where  $A(1) = 1/6$  and  $A(w)$  diverges if  $w \rightarrow 0$  (data not shown).

We conclude this section with the following observation, which is necessary for the consistency of the present model for avalanches. If one looks at the expression (59) of the average (over configurations) probability that a tile hitting the interface is reflected, one sees that for small values of  $w$ , the probability approaches the value one. This implies that to obtain large avalanches (small  $\tau$ ) one has to wait a long time. This is to be expected in models of SOC.

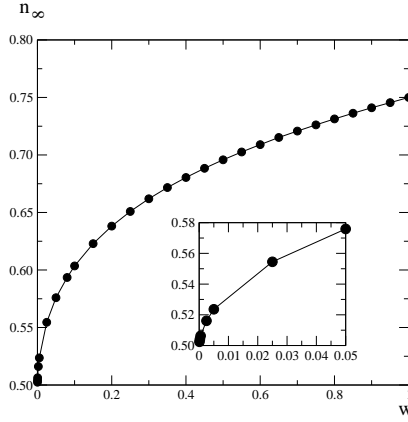


**Figure 20.** The  $w$  dependence of the fraction of the interface where adsorption does not take place  $n_\infty$  obtained from the extrapolated results of Monte Carlo simulations.

$w$	$L$	$n_L$	$\langle T \rangle_L$	MF	$\langle T \rangle_L/\text{MF}$
1	1024	0.749	1.497	1.497	0.999
1	2048	0.749	1.498	1.501	0.998
1	4096	0.749	1.499	1.500	0.998
1	8192	0.749	1.499	1.499	0.999
0.00025	1024	0.199	496.999	496.119	1.001
0.00025	2048	0.313	914.346	913.820	1.001
0.00025	4096	0.407	1374.713	1373.856	1.001
0.00025	8192	0.455	1674.877	1674.550	1.000

**Table 4.** Values of  $n_\infty$  and the average number of tiles obtained from Monte Carlo simulations  $\langle T \rangle_L$  as compared with the mean-field results (MF). The values are given for several lattice sizes  $L$  and two values of  $w$ :  $w = 1$  and  $w = 0.00025$ .

## 8. Conclusions

We have shown that the one parameter  $u = 1/w$  dependent RPM has an unusual phase diagram (see Fig. 10). At  $u = 1$  (the Razumov-Stroganov point) the model has many facets. Firstly, the stationary state is related to a two-dimensional equilibrium system. The details of this observation are still at the level of a conjecture. The fact that the normalization factor of the stationary PDF is related to an enumeration problem of a two-dimensional system (fully packed loops or alternating sign matrices) was recently proved rigorously [48]-[50]. The two-dimensional system has many interesting combinatorial properties which are reflected in the PDF of the stationary state. Also at  $u = 1$  the Markov process has a space-time symmetry (conformal invariance) which does not exist for  $u \neq 1$ .

How does the combinatorial facet of the model can be used to derive meaningful physical quantities? Using small system sizes, one can "guess" expressions which can be checked by Monte-Carlo for large systems. One example is the probability to have  $k$  clusters for a system of size  $L = 2n$  (see Eq. (44)). Actually this expression is a solution

of some bilinear recurrence relations (Pascal hexagon [18]). For another example, see Eq. (58).

The conformal invariance facet of the model has other consequence. It fixes the value of the dynamical critical exponent:  $z = 1$ . It also fixes the finite-size scaling behavior of the density of contact points (see Eqs. (47) and (48)), the form of the two-contact point correlation function (see Fig. 17) and the Family-Vicsek scaling functions (see Eq. (53) and Fig. 16(b)).

The RPM has been extended in several directions. In one of them, one has kept the Hamiltonian (28) but enlarged the vector space on which it acts to a larger left ideal. This has allowed us [51], keeping conformal invariance, to study the move of a random walker in an unquenched disordered system as well as the annihilation reaction  $A + A \rightarrow \emptyset$  in the same medium. The same study for other models, without conformal invariance, can be found in [52] and [53].

Some very interesting results have been obtained by extending the TL semigroup algebra to the one-boundary TL semigroup algebra [17]-[19]. The configuration space is different and biased toward the one end of the system where a new generator is placed. The model gets new combinatorial facets and conformal invariance is maintained.

Before closing this paper, we would like to comment on the phase diagram of the RPM (see Fig. 10). If we perturb the system and go away from  $u = 1$ , one obtains a massive phase if  $u < 1$ . This happens with many conformal invariant models. If however we take  $u > 1$ , the system stays scale invariant with varying critical exponents without being conformal invariant. This phenomenon is new and it is a consequence of the nonlocality of the model [54]. From a phenomenological point of view we think that the observation that for any finite  $u$  the average height stays finite for large lattice sizes is very unexpected (for unweighted RSOS paths it increase like  $L^{1/2}$ ). Keeping in mind that for  $w = 0$ , in the stationary state, there exists only one configuration which is a full triangle (see Fig. A2) one is tempted to believe that configurations where on "feels" the triangle effects should play an important role. This is not the case (see Fig. 15).

## Acknowledgments

This work was supported in part by FAPESP and CNPq (Brazilian Agencies), by the Deutsche Forshungsgemeinschaf (Germany), and by The Australian Research Council.

## Appendix. Link diagrams and RSOS (Dick) paths

We consider a one-dimensional lattice with  $L+1$  ( $L = 2n$ ) sites. The configuration space of the fluctuating interface is given by RSOS paths (better known in combinatorics as Dick paths). They are defined by taking nonnegative heights  $h_i$  which obey the restricted solid-on-solid (RSOS) rules

$$h_{i+1} - h_i = \pm 1, \quad h_0 = h_L = 0, \quad h_i \geq 0. \quad (\text{A.1})$$

See Fig. A2 for an example.

Each RSOS path corresponds to a link pattern (see section 3) in the following way. On each RSOS path, draw the equal height contour lines as in Fig. A1a. By straightening out the surface, keeping the contour lines and rotating the picture around the horizontal axis, we obtain Fig. A1b. The contour lines connect pairs of sites and Fig. A1b defines a link pattern. Notice than for an RSOS path defined on  $L + 1$  sites corresponds a link pattern defined on  $L$  sites.

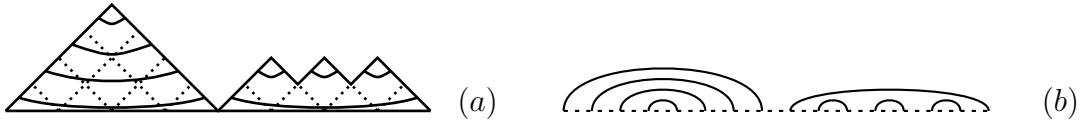


**Figure A1.** An interface with contour lines (a) and the corresponding link pattern (b).

In the case  $L = 6$  for example, to the five link patterns (29) correspond five RSOS configurations

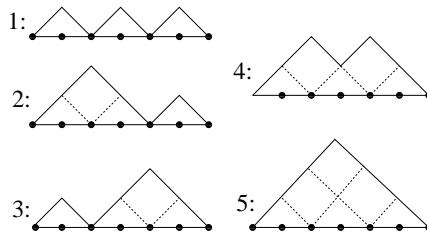


**Figure A2.** The RSOS configurations corresponding to the links patterns (29) of the  $L = 6$  lattice ( $(L + 1)$  points).

One can read off the action of the Hamiltonian (30) on this configuration space and therefore get the different transition rates. These are the transition rates of the RPM at the Razumov-Stroganov point used in Section 5.

## References

- [1] de Gier J, Nienhuis B, Pearce P and Rittenberg V, 2004 *J. Stat. Phys.* **114** 1
- [2] Alcaraz F C, Levine E and Rittenberg V, 2006 *J. Stat. Mech.* P08003
- [3] de Gier J, Nienhuis B, Pearce P A and Rittenberg V, 2003 *Phys. Rev. E* **67** 016101
- [4] Batchelor M T, de Gier J and Nienhuis B, 2001 *J. Phys. A: Math. Gen.* **34** L265
- [5] Pearce P A, Rittenberg V, de Gier J and Nienhuis B, 2002 *J. Phys. A: Math. Gen.* **35** L661
- [6] Elkies N, Kuperberg G, Larsen M and Propp J, 1992 *J. Algebraic Combin.* **1**
- [7] Batchelor M T, Blöte H W, Nienhuis B and Yung CM, 1996 *J. Phys. A: Math. Gen.* **29** L399  
111; 219-234
- [8] de Gier J, 2005 *J. Discr. Math.* **298** 365
- [9] Bressoud D M, 1999 *Proofs and Confirmations: The story of the Alternating Sign Matrix Conjecture* (Cambridge, Cambridge Press)
- [10] Razumov A V and Stroganov Yu G, 2001 *J. Phys. A: Math. Gen.* **34** 3185
- [11] Razumov A V and Stroganov Yu G, 2004 *Theor. Math. Phys.* **138** 333

Razumov A V and Stroganov Yu G, 2004 *Theor. Math. Phys.* **138** 395

[12] Razumov A V and Stroganov Yu G, 2005 *Theor. Math. Phys.* **142** 237  
Razumov A V and Stroganov Yu G, 2005 *Theor. Mat. Phys.* **142** 284

[13] Di Francesco P, Mathieu P, and Senechal F, 1991 *Conformal Field Theory*, (Springer-Verlag: New York)

[14] Temperley H N V and Lieb E, 1971 *Proc. R. Soc. London A* **322** 251

[15] Martin P, 1991 *Potts models and related problems in statistical mechanics*, Series on Advances in Statistical Mechanics - v. 5, (Singapore: World Scientific)

[16] Dhar D, 1999 *Preprint* cond-mat/9909009

[17] Martin P, Saleur H, 1993 *Commun. Math. Phys.* **158** 155

[18] Pyatov P, 2004 *J. Stat. Mech.* P09003

[19] de Gier J, Nichols A and Rittenberg V, 2005 *J. Stat. Mech.* P03003

[20] Alcaraz F C, Pyatov P and Rittenberg V, in preparation

[21] Bish D and Jones V, 1997 *Inv. Math.* **128** 89

[22] Di Francesco P, 1998 *Nucl. Phys. B* **532** 609

[23] Batchelor M T, de Gier J and Nienhuis B, 2002

[24] Martins M J and Ramos P B, 1997 *Nucl. Phys. B* **500**, 579

[25] Martins M J, Nienhuis B and Rietman R, 1998 *Phys. Rev. Lett.* **81** 504

[26] de Gier J and Nienhuis B, 2005 *J. Stat. Mech.* P01006

[27] Pasquier V and Saleur H, 1990 *Nucl. Phys. B* **330** 523

[28] Alcaraz F C, Barber M N, Batchelor M T, Baxter R J and Quispel G R W, 1987 *J. Phys. A: Math. Gen.* **20** 6397  
Alcaraz F C, Barber M N and Batchelor M T, 1988 *Ann. Phys., NY* **182** 280

[29] Bauer M and Saleur H, 1989 *Nucl. Phys. B* **320** 591

[30] Baxter R J, 1982 *Exactly solved models in statistical mechanics*, (Academic Press: London)

[31] Korepin V E, 1982 *Comm. Math. Phys.* **86** 391 *Int. J. Mod. Phys. B* **16** 1883

[32] Kuperberg G, 2002 *Ann. of Math.* **156** 835

[33] Burkhardt T W and Xue T, 1991 *Phys. Rev. Lett.* **66** 895

[34] Flohr M, private communication

[35] Bouwknegt P and Schoutens K, 1993 *Phys. Rep.* **223** 183

[36] Bauer M, private communication

[37] Bauer M and Bernard D, 2003 *Commun. Math. Phys.* **239** 493

[38] Arndt P F and Heinzel T, 1995 *J. Phys. A: Math. Gen.* **28** 3567

[39] Family F and Vicsek E, 1985 *J. Phys. A: Math. Gen.* **18** L75

[40] We thank the referee of this paper for this nice observation

[41] Bak P, Tang C and Wiesenfeld K, 1988 *Phys. Rev. A* **38** 364

[42] Dhar D and Ramaswamy R, 1989 *Phys. Rev. Lett.* **63** 1659

[43] Dhar D, 1999 *Physica A* **263** 4

[44] Tebladi C, De Menech M and Stella A L, 1999 *Phys. Rev. Lett.* **83** 3952

[45] Priezzhev V B, Ivashkevich E V, Povolotsky A M and Hu C K, 2001 *Phys. Rev. Lett.* **87** 084301

[46] Dhar D, private communication

[47] Stroganov Yu G, private communication

[48] Pasquier V, 2006 *Ann. Henri Poincaré* **7** 397

[49] Di Francesco P and Zinn-Justin P, 2005 *Electron. J. Comb.* **12** R6

[50] Di Francesco P and Zinn-Justin P, 2005 *J. Phys. A: Math. Gen.* **38** L815

[51] Alcaraz F C and Rittenberg V, 2006 *Preprint* cond-mat/0612272

[52] Kissinger T, Kotowicz A, Kurz O, Ginelli F, and Hinrichsen H, 2005 *J. Stat. Mech.* P06002

[53] Ginelli F, Hinrichsen H, Livi R, Mukamel D, Torcini A, 2006 *J. Stat. Mech.* P08008

[54] Riva V and Cardy J, 2005 *Phys. Lett. B* **622** 339